Advanced Chemical Engineering

ADVANCED CHEMICAL ENGINEERING Open Access

www.advchemeng.com

RESEARCH ARTICLE OPEN ACCESS

Tunable Anodes: A Dynamic Solution for Fluctuating Green Electricity

Mojtaba Mohseni[1] | Jonas Baessler[1] | Alexander Kohushoelter[1] | Georgia Ioanna Prokopou[2] | Alexander Mitsos[2] | Matthias Wessling[1,3] | Robert Keller[1]

[1]RWTH Aachen University, Aachener Verfahrenstechnik - Chemical Process Engineering (AVT.CVT), Aachen, Germany | [2]RWTH Aachen University, Aachener Verfahrenstechnik - Process Systems Engineering (AVT.SVT), Aachen, Germany | [3]DWI - Leibniz Institute for Interactive Materials, Aachen, Germany

Correspondence: Robert Keller (robert.keller@avt.rwth-aachen.de)

Received: 7 April 2026 | **Revised:** 30 June 2026 | **Accepted:** 7 July 2026

Keywords: demand-side management | dynamic electrolysis | hydrogen oxidation reaction (HOR) | oxygen evolution reaction (OER) | tunable anode

ABSTRACT

Time-variable electricity prices from intermittent solar and wind motivate flexible, price-responsive electrochemical operation. In emerging electrosynthesis platforms, such as CO_2RR, demand-side management relies on oversized cells and product storage during peak-cost periods. We introduce a switchable and tunable anode architecture that modulates cell voltage (and thus power draw) without oversizing the electrolyzer. The two-chamber anode separates HOR (hydrogen oxidation reaction) and OER (oxygen evolution reaction) compartments by a cation-exchange membrane (CEM), enabling rapid mode changes between low-overpotential HOR and conventional OER without a rinsing or shutdown step. We demonstrate 120 stable switching cycles at 100 mA cm^{-2}. Beyond binary switching, the architecture enables simultaneous HOR/OER operation (0%–100% split), providing continuous control of anode potential and power demand at constant cathodic current density. In a representative conservative electricity-price scenario, the tunable strategy yields up to 22.6% lower anodic operating cost than conventional OER. This study provides a new operational degree of freedom in electrochemical systems, focusing on the feasibility and controllability of dynamic anodic modulation. More broadly, the concept establishes continuous counter-electrode tuning as a new lever for flexible electrochemical process design, enabling real-time adjustment of power demand without altering the target reaction rate.

1 | Introduction

The integration of wind and solar power into the grid leads to fluctuating electricity prices [1, 2]. Demand-side management (DSM) adjusts process operation in response to these price signals [3, 4]. For electrochemical processes, this motivates operating strategies that can modulate power draw on demand while maintaining a constant production-side operating point.

A conventional DSM approach in electrolysis is to oversize cells and buffer products or intermediates during high-price periods [2]. For chlor–alkali (CA) electrolysis and the carbon dioxide reduction reaction (CO_2RR), however, storing hazardous gases (e.g., Cl_2, CO) introduces substantial safety risks and costs [5, 6]. Therefore, DSM concepts that directly lower cell voltage—rather than relying on product buffering—are particularly attractive for such systems.

One route to reduce cell potential on demand is to switch the anode or cathode reaction. In CA, the anode evolves chlorine, and NaOH forms via the cathodic hydrogen evolution reaction (HER); alternatively, using the oxygen reduction reaction (ORR) at the

Mojtaba Mohseni and Jonas Baessler contributed equally to this work.

This is an open access article under the terms of the Creative Commons Attribution License, which permits use, distribution and reproduction in any medium, provided the original work is properly cited.
© 2026 The Author(s). *Advanced Chemical Engineering* published by Wiley-VCH GmbH.

cathode can maintain NaOH production at a lower cell potential. This enables cathode-side DSM with a bifunctional cathode [1, 7] via switchable oxygen-depolarized cathode (sODC) operation [8]

$$2H_2O + 2e^- \rightarrow H_2 + 2OH^- \quad (\mathrm{HER}, E^0 = 0.0\,\mathrm{V}, H_2\ \mathrm{mode}, \mathrm{cathode}) \tag{1}$$

$$2H_2O + O_2 + 4e^- \rightarrow 4OH^- \quad (\mathrm{ORR}, E^0 = 0.4\,\mathrm{V}, O_2\ \mathrm{mode}, \mathrm{cathode}) \tag{2}$$

$$2H_2O \rightarrow O_2 + 4H^+ + 4e^- \quad (\mathrm{OER}, E^0 = 1.23\,\mathrm{V}, O_2\ \mathrm{mode}, \mathrm{anode}) \tag{3}$$

$$H_2 \rightarrow 2H^+ + 2e^- \quad (\mathrm{HOR}, E^0 = 0.0\,\mathrm{V}, H_2\ \mathrm{mode}, \mathrm{anode}) \tag{4}$$

In sODC, the cathode toggles between HER (H_2 mode, higher energy) and ORR (O_2 mode, lower energy) in response to price fluctuations [8], reducing electricity demand by 33% when switching to O_2 mode [9]. This illustrates a central DSM principle: replacing a high-overpotential counter-reaction with a lower-overpotential alternative while keeping the desired product formation unchanged.

Dual-mode operation has also been explored in electrochemical energy-conversion and storage systems beyond industrial electrolysis. For example, Bai and coworkers [10] reported a rechargeable lithium–bromine/oxygen fuel cell in which the cathode-side reaction could be switched from oxygen reduction in aqueous media, including seawater, to bromine reduction in a bromine-containing catholyte. This change in catholyte and reaction pathway enabled an on-demand increase in power output, illustrating how alternative electrode reactions can be activated dynamically to overcome kinetic or transport limitations under specific operating conditions. Such dual-mode fuel-cell and flow-battery-inspired concepts demonstrate the broader value of electrochemical architectures that adapt their dominant electrode reaction to the required power profile.

For cathodic production processes such as CO_2RR or electrogeneration of H_2O_2, however, the desired products form at the cathode working electrode (WE), which is conventionally paired with anodic OER (1.23 V, Equation (3)) [11]. Replacing OER with HOR (0.0 V, Equation (4)) can, in principle, lower the cell voltage by 1.23 V without decreasing the cathodic production rate. HOR (i.e., a hydrogen-depolarized anode, HDA; also referred to as a hydrogen diffusion/consuming anode) has been explored in related electrochemical platforms, including membrane electrolysis [12, 13], salt splitting [14, 15], and electrochemical H_2O_2 synthesis [16]. To date, to the best of our knowledge, switching—and continuously tuning—between HOR and OER within a single anode module has not been reported. Translating OER/HOR modulation into practical DSM therefore requires an architecture that enables rapid, safe transitions as well as continuous adjustment between modes.

A key challenge for reaction-switching DSM is that transitions between O_2- and H_2-related modes can form explosive O_2/H_2 mixtures in electrolyzer gas compartments [1, 8]. Safety protocols therefore require power shutdown and inert-gas rinsing before mode changes [1, 8], leading to downtimes of up to 30 min per switch [2]. These delays limit the achievable switching frequency and, in turn, reduce the practical value of DSM, motivating designs that eliminate rinsing while maintaining safe operation. Moreover, current bifunctional cathodes cannot operate in O_2 and H_2 modes simultaneously due to explosion risk [7, 8]. Enabling simultaneous operation with independently adjustable contributions would provide continuous, fine-tuned energy control—particularly relevant because electricity prices often vary gradually rather than in purely binary "cheap/expensive" intervals.

In this work, we introduce a switchable and tunable anode module that leverages O_2- and H_2 modes by integrating two anodes separated by a cation-exchange membrane (CEM), as depicted in Figure 1. We consider gas crossover through the CEM and evaluate it experimentally. By physically separating the reaction compartments, the architecture enables mode transitions without a rinsing or shutdown step, addressing a key practical bottleneck of gas-switching concepts. Beyond binary switching, the design supports simultaneous HOR/OER operation with a continuously adjustable split, providing a continuous "dial" to tune anode potential and power demand at constant cathodic current density. This separation also decouples the HOR catalyst from OER potentials, avoiding the large potential excursions implicated in the degradation of bifunctional ORR/OER electrodes [17, 18].

The objective of this study is to establish the feasibility and controllability of the architecture as an enabling concept for dynamic electrochemical operation, rather than to optimize performance metrics such as maximum current density or long-term durability, which are expected to depend on the specific cell design and application. In this sense, the proposed design introduces a new operational degree of freedom: electrical energy demand can be modulated dynamically without altering the production-side operating point. We validate the concept experimentally through switching and tunability tests and demonstrate its process-level relevance via an optimization-based operating-cost analysis under a representative electricity-price profile.

2 | Experimental

2.1 | Materials

Potassium sulfate (K_2SO_4, ≥99%) was purchased from VWR. Sodium sulfate (Na_2SO_4, ≥99%), sulfuric acid (H_2SO_4, ≥95%), and platinum on graphitized carbon (20 and 40 wt% Pt/C) were purchased from Sigma–Aldrich. The PFSA ionomer solution (Fumion FLN-905) was purchased from Fumatech.

2.2 | Module Configuration

Figure S1 illustrates the anode side of the flow-through module (Flex-E-Cell, FXC Engineering GmbH) used in the experiments. H_2 gas flowed through a meander-shaped titanium flow frame that contacted the first anode for HOR (HOR-anode) and served

3053786x, 2026, 1, Downloaded from https://advanced.onlinelibrary.wiley.com/doi/10.1002/ache.70003 by Universitatsbibliothek RWTH Aachen University, Wiley Online Library on [30/09/2026]. See the Terms and Conditions (https://onlinelibrary.wiley.com/terms-and-conditions) on Wiley Online Library for rules of use; OA articles are governed by the applicable Creative Commons License

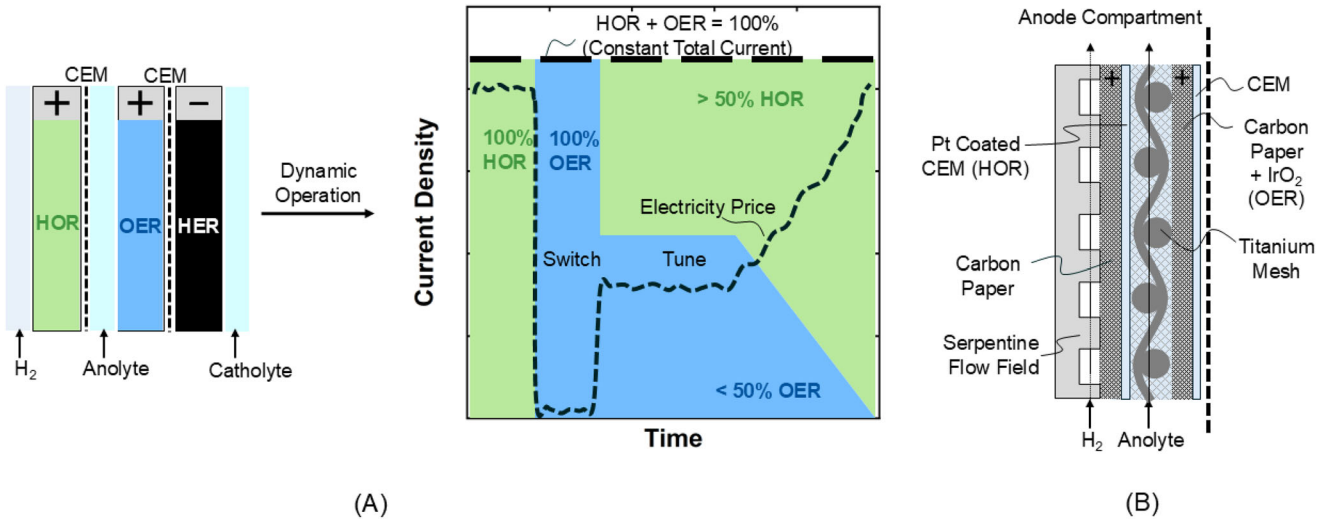


FIGURE 1 | Schematic of the switchable/tunable anode concept and cell architecture. (A) Illustration of the dynamic anode strategy for adapting operation to electricity price fluctuations arising from a growing share of renewable energy. (B) Tunable anode configuration including a serpentine H_2 flow field, carbon-paper gas diffusion layer (GDL), Pt-coated cation-exchange membrane (CEM) separating the anode chambers, titanium-mesh current collector, and IrO_2-coated carbon paper as the oxygen evolution reaction (OER) electrode.

as a current collector. The HOR-anode was a gas diffusion electrode (GDE) comprising a commercial carbon paper gas diffusion layer (CP; Sigracet 39BB, Fuel Cell Store) in contact with a homemade catalyst-coated membrane (CCM). The CCM was prepared using a film coater (FOM Technologies) with a wet film thickness of 50 µm, a substrate speed of 0.3 m min^{-1}, a coating distance of 150 µm, and a substrate-bed temperature of 50°C. Nafion 115 was used as the membrane and coated with 0.25 mg cm^{-2} Pt/C (40 wt%) as the catalyst. We selected Pt as the HOR catalyst because it provides benchmark HOR kinetics in acidic media (Pt > Ir > Rh > Pd), enabling a clear upper-bound proof-of-principle for voltage reduction via HOR assistance [19, 20].

An anolyte of 2 M H_2SO_4 was pumped through a second flow frame filled with a spacer, which contacted the second anode for OER (OER-anode). A hydrophilized GDE (5 × 5 cm) was airbrushed with an iridium oxide catalyst ink (IrO_2 nanoparticles, isopropanol, and Nafion) [21] to a target loading of 2 mg cm^{-2} and used as the OER-anode. A titanium foam served as the current collector for the second anode. As the next layer, a second CEM (Nafion 117, Fumatech) separated the OER-anode from the cathode compartment. A commercial gas diffusion layer (Sigracet 39BB, Fuel Cell Store) was airbrushed with 20 wt% Pt/C to a loading of 1 mg cm^{-2} [22] and served as the cathode. For proof-of-principle experiments, the cathode was contacted with 1 M H_2SO_4 to perform HER; note that HER can be replaced by other cathodic reactions such as CO_2RR.

2.3 | Experimental Setup

Figure S2 depicts the anode-side experimental setup. Before entering the module, H_2 or N_2 (100 sccm) was humidified by passing it through a water column. At the outlet, the gas stream was routed through a gas cooler and then to O_2- and H_2-analyzers. The anolyte (2 M H_2SO_4) was preheated in a heat exchanger to 60 °C before entering the electrochemical module. The cell effluent was directed to a phase separator to remove bubbles generated by OER. The anolyte was operated in a feed-and-bleed mode [23] with circulation and feed flow rates of 50 and 2 mL min^{-1}, respectively. The reference electrode (RE) was placed in the anolyte stream upstream of the module inlet. The catholyte was circulated at 50 mL min^{-1}. The HOR and OER anodes served as working electrodes and could be controlled either dependently or independently.

2.4 | Model Description

A spatially lumped, quasi-steady, discrete-time model of the operating strategies was implemented in GAMS 44.1.0 and solved as an MIQP/QP using Gurobi [24] to minimize anodic operating cost via switching/tuning. The tuning outcome depends on the assumed prices: deionized water at 0.6 € t^{-1} [25, 26], electricity from a 1 h-resolution weekly price profile for 2022 (Figure 4A) based on Papadimitriou et al. [27] that exhibits large fluctuations consistent with increasing variable-renewable penetration, and hydrogen at 8 € kg^{-1} [28]. The hydrogen price represents a conservative scenario consistent with techno-economic projections for near-term hydrogen supply chains [29] and encompasses production, balance-of-plant, transportation, and dispensing costs.

3 | Results and Discussion

As illustrated in Figure 1A, electricity prices often vary gradually; therefore, continuously tuning the contribution of each anode can exploit price signals more effectively than binary switching alone. When H_2 is used as the feedstock/fuel in H_2 mode, its availability and price provide an additional control variable for selecting the operating split. Accordingly, rapid switching combined with continuous fraction control provides a versatile

3053786x, 2026, 1, Downloaded from https://advanced.onlinelibrary.wiley.com/doi/10.1002/ache.70003 by Universitatsbibliothek RWTH Aachen University, Wiley Online Library on [30/09/2026]. See the Terms and Conditions (https://onlinelibrary.wiley.com/terms-and-conditions) on Wiley Online Library for rules of use; OA articles are governed by the applicable Creative Commons License

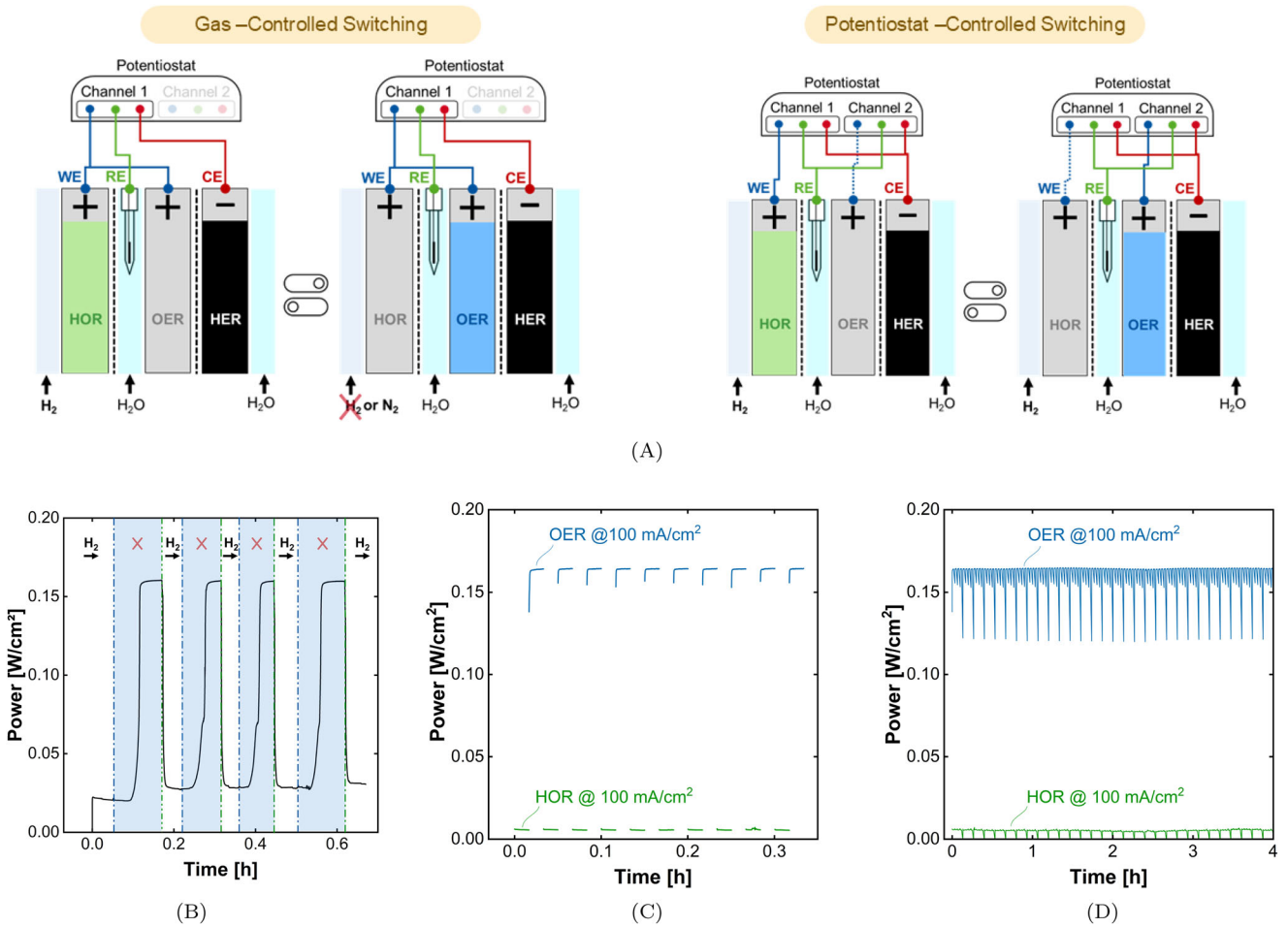


FIGURE 2 | HOR/OER switching experiments at a constant cathodic current density of 100 mA cm^{-2}. (A) Schematic of the two switching modes employed: gas- and potentiostat-controlled modes. (B) Reversible switching between HOR and OER by toggling the H_2 feed in the gas-controlled mode. (C,D) Reversible switching in potentiostat-controlled mode for 10 and 120 cycles, respectively, independent of the gas supply.

framework for flexible operation in response to both electricity and feedstock (e.g., H_2) price dynamics.

Figure 1B schematically illustrates the tunable anode configuration, in which a Pt-coated CEM separates the HOR compartment from the OER compartment. During HOR mode, the anolyte (H_2SO_4) was circulated to maintain ionic conductivity. Switching between H_2-mode (HOR-anode) and O_2-mode (OER-anode) can be implemented in two ways: gas-controlled and potentiostat-controlled operation (Figure 2A). In the gas-controlled approach, the HOR- and OER-anodes are connected to a single potentiostat channel, and the operating mode is determined by H_2 availability because HOR exhibits a lower overpotential and faster kinetics than OER. Because the two anodes are electrically connected, the measured anode potential corresponds to a single shared node potential and fluctuates between ~ 0.2 V (HOR-dominated) and ~ 1.6 V (OER-dominated) (same trace as Figure 2B). Consequently, the Pt-based HOR electrode can be repeatedly driven between reduced and oxidized states during OER periods. Although PtO_x formation is reversible upon returning to HOR, such metal/oxide cycling is known to accelerate Pt dissolution and corrosion compared with operation at a constant high potential where a passive oxide layer forms [30]. Similar potential-window cycling challenges have been widely discussed for unitized regenerative fuel cells (URFCs) and related reversible electrochemical devices [31]. By contrast, in potentiostat-controlled operation, each anode is connected to a separate potentiostat channel, allowing the HOR and OER contributions to be adjusted independently. In this configuration, the HOR electrode potential can be held in the HOR regime, keeping the Pt catalyst in a reduced state and avoiding the redox cycling that drives transient dissolution and corrosion.

In the gas-controlled approach, switching was implemented either by turning the H_2 supply on and off (Figure 2B) or by replacing H_2 with N_2 (Figure S4). In our configuration, the IrO_2 electrode operates in the anolyte-fed OER compartment and is not exposed to the H_2/N_2 gas stream; therefore, gas switching directly controls the HOR compartment. Accordingly, the power consumption remains at approximately 0.02 W cm^{-2} in HOR mode and increases to 0.16 W cm^{-2} in OER mode after turning off the H_2 supply (Figure 2B) or switching to N_2 (Figure S4). A short response delay was observed: 2–3 min for H_2 on/off switching (Figure 2B) and 5–10 min for H_2/N_2 switching (Figure S4). The longer delay in the H_2/N_2 experiments can be attributed to the time required to exchange 300–600 mL of gas within the humidifier. The response time could be reduced by switching between H_2 and N_2 directly at the cell inlet, as the delay is expected to depend

3053786x, 2026, 1, Downloaded from https://advanced.onlinelibrary.wiley.com/doi/10.1002/ache.70003 by Universitatsbibliothek RWTH Aachen University, Wiley Online Library on [30/09/2026]. See the Terms and Conditions (https://onlinelibrary.wiley.com/terms-and-conditions) on Wiley Online Library for rules of use; OA articles are governed by the applicable Creative Commons License

on the residence-time distribution of the gas stream. Overall, these response times are compatible with frequent demand-side adjustments and avoid the long downtime typically associated with shutdown and inert-gas rinsing in gas-switching concepts.

Notably, upon switching back from N_2 to H_2 (Figure S4), the power drops sharply and then decreases more slowly to the steady HOR value. This behavior is consistent with a short conditioning step, for example, reduction of PtO_x formed while the electrically connected anode node was at OER-level potentials. Although oxide reduction restores HOR activity, repeated cycling between oxidized and reduced states can accelerate cumulative Pt dissolution during long-term operation [30, 31]. By contrast, in the potentiostat-controlled configuration (Figure 2C,D), independent potential control maintains the HOR electrode in the HOR regime, minimizing such transients and mitigating corrosion by design.

Additionally, H_2 was continuously supplied to the HOR anode during potentiostat-controlled switching, enabling rapid transitions between the two modes, as shown in Figure 2C and Figure 2D for 10 and 120 switching events, respectively. Stable operation was observed in both HOR and OER modes, indicating that the system maintains its switching behavior over repeated cycling at 100 mA cm^{-2}. The experiments were intentionally conducted at a moderate current density to isolate and validate the switching characteristics of the tunable-anode architecture under well-controlled conditions. Extending operation to higher current densities is expected to introduce additional transport, ohmic, and thermal effects and thus represents an important target for future engineering optimization rather than a limitation of the switching principle itself.

Given the additional CEM separating the HOR and OER anodes (Figure 1B) and the absence of a rinsing requirement due to negligible O_2 crossover into the H_2 gas channel (Figure S3), we investigated whether the HOR and OER contributions can be tuned independently while maintaining a constant cathodic current density of 100 mA cm^{-2}. As shown in Figure 3A, the current densities of the HOR (green) and OER (blue) anodes were initially set to 50 mA cm^{-2} each and then adjusted stepwise to 100 and 0 mA cm^{-2}, respectively. Figure 3B shows the corresponding specific power demand of the HOR anode, the OER anode, and their sum. Importantly, this provides a continuous "dial" of power demand at constant cathodic current density, that is, without changing the production-side operating point.

Accordingly, the total power demand starts at 0.078 W cm^{-2} and decreases stepwise to a minimum of 0.027 W cm^{-2} as the HOR share increases to 100%. In contrast, the total demand increases to 0.16 W cm^{-2} when the OER anode reaches a 100% contribution. The anode potentials (Figure 3C) of the HOR and OER anodes also change stepwise over time. In 100% O_2 mode, the HOR-anode potential is close to 0 V versus RHE because it is inactive and outside the electrical field (Figure 1B). In 100% H_2 mode, by contrast, the OER-anode potential remains above 0 V versus RHE (Figure 3C). This behavior reflects the compartment design: when the HOR anode is activated, it brings the adjacent OER compartment into the electrical field (Figure 1B). Nonetheless, no OER occurs in 100% H_2 mode because the WE potential of the OER anode remains below its standard potential of 1.23 V Equation (3).

The cell potential (Figure 3D) is the WE–CE difference, measured separately for the HOR and OER anodes. In HOR mode, it additionally includes the ohmic drop across the extra CEM separating the HOR and OER anodes (Figure 1B). At 100% HOR and 100% OER, the cell potentials are ~0.6 and ~1.7 V, respectively; that is, switching to HOR saves ~1.1 V. HOR mode thus consumes H_2 to reduce electrical energy demand. As a reference, HOR mode and proton-exchange membrane fuel cells (PEMFCs) consume H_2 at the same rate at a given current density; however, the tunable anode exploits HOR without the cathodic ORR, which dominates fuel-cell losses [32]. State-of-the-art PEMFCs deliver ~0.8 V at 100 mA cm^{-2} [33], about 0.3 V lower than the potential saved by switching, underscoring switchable/tunable anodes as efficient, highly dynamic hydrogen-to-power buffers.

At higher current densities, the quantitative performance of the present architecture is expected to be increasingly influenced by additional ohmic losses across the extra CEM, as well as by mass-transport and gas-management effects in the dual-anode configuration. These aspects represent engineering optimization challenges rather than conceptual limitations of the switching/tuning principle and should be addressed in future scale-up studies. The concept could also extend to electrochemical systems in which two target reactions have distinct optimal potentials or production rates. In electro-Fenton, for example, the optimal potential for H_2O_2 generation via ORR differs from that for Fe^{2+} regeneration, constraining overall efficiency [34, 35].

Gas crossover between electrodes was evaluated by operating in OER mode while purging the back side of the HOR anode with N_2 (instead of H_2) and monitoring O_2 transport through the CEM into the H_2 gas channel. As shown in Figure S3, no O_2 was detected at an N_2 flow of 100 sccm; reducing the N_2 flow to 50 sccm increased the O_2 fraction to a maximum of 0.02%. Thus, under these conditions, the CEM effectively suppressed O_2 crossover to the H_2 channel during electrolysis at 100 mA cm^{-2}. Because the present work represents a first reactor-level demonstration of the concept, a comprehensive assessment at higher current densities and with CEMs of varying thickness and chemistry will be required in future studies.

In PEM water electrolysis, hydrogen crossover to the anode (H_2-in-O_2) can be more severe than transport in the reverse direction and may raise efficiency and flammability concerns when both compartments sustain substantial gas phases, particularly with thin membranes, under dynamic operation, or under differential-pressure conditions [36–38]. One key contributor discussed for PEM electrolysis is HER-induced H_2 supersaturation in the cathode catalyst layer, which can increase the driving force for H_2 permeation [39]. In the present architecture, however, the H_2 compartment operates in HOR mode and therefore consumes H_2 rather than generating it, such that HER-driven H_2 supersaturation is intrinsically absent. Moreover, the OER anode is polarized positive of the HOR equilibrium potential, so permeated H_2 is expected to be oxidized immediately rather than accumulate. Accordingly, we focused experimentally on the safety-relevant direction for our configuration, that is, O_2 crossover into the H_2 gas channel.

3053786x, 2026, 1, Downloaded from https://advanced.onlinelibrary.wiley.com/doi/10.1002/ache.70003 by Universitatsbibliothek RWTH Aachen University, Wiley Online Library on [30/09/2026]. See the Terms and Conditions (https://onlinelibrary.wiley.com/terms-and-conditions) on Wiley Online Library for rules of use; OA articles are governed by the applicable Creative Commons License

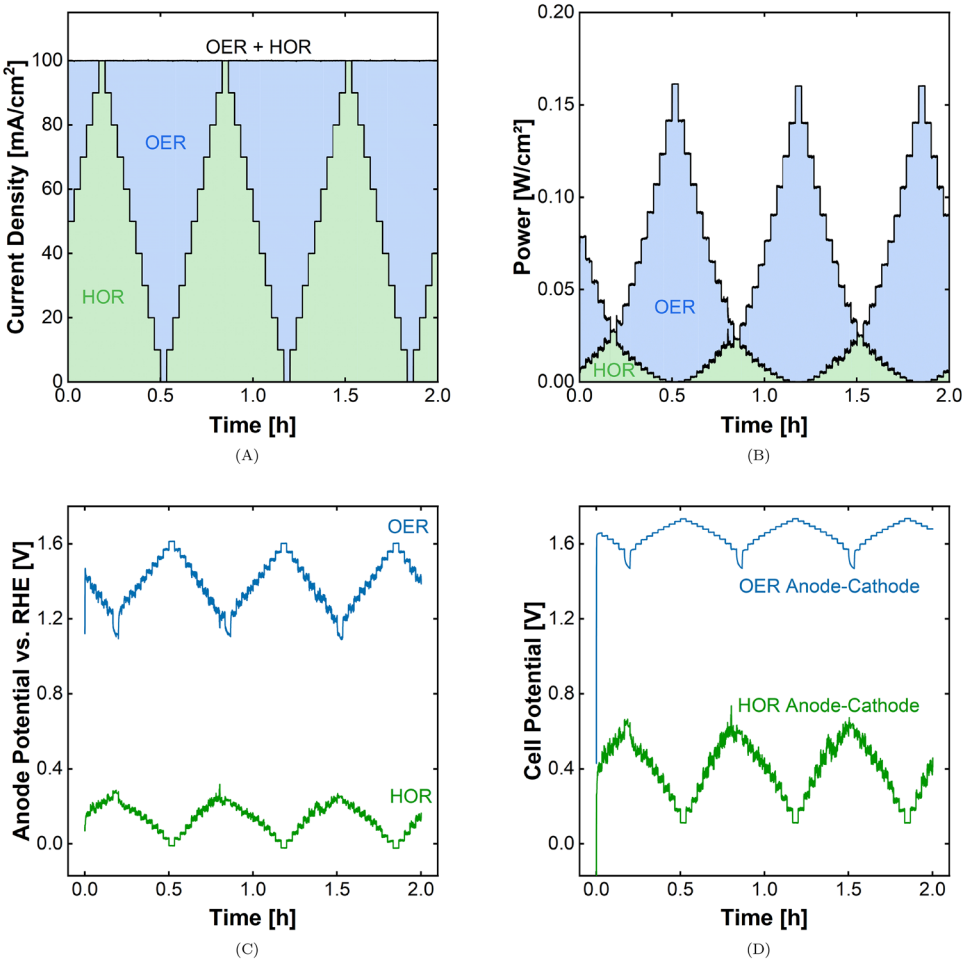


FIGURE 3 | Tuning experiments with variable HOR and OER contributions, each adjusted between 0 and 100 mA cm^{-2}, while maintaining a constant cathodic current density of 100 mA cm^{-2}. (A) Current-density profile applied to the HOR and OER modes, starting from 50 mA cm^{-2} in each mode and followed by stepwise cyclic increases and decreases. (B) Corresponding tunable power consumption of the electrolysis cell under constant cathodic operation. (C) Measured anode potential. (D) Calculated cell potential ($E_{\text{Anode}} - E_{\text{Cathode}}$) for the different HOR/OER contributions.

Furthermore, our model-based optimization evaluates the potential of switchable and tunable operation (Figure 1) to reduce operating costs under a fluctuating electricity-price profile, compared with conventional OER operation, similar to Brée et al. [1]. Four strategies are defined: (i) operation exclusively in hydrogen mode (HOR); (ii) switchable operation with rinsing between HOR and OER modes [1, 8] (SWITCH-R); (iii) switchable operation without rinsing enabled by our design (Figure 2A, SWITCH-NR); and (iv) tunable operation with simultaneous HOR/OER (TUNE).

Using the representative weekly electricity-price profile in Figure 4A, Figure 4B depicts the relative anodic operating cost of HOR, SWITCH-R, SWITCH-NR, and TUNE compared with OER. All four alternatives yield lower anodic operating costs than OER. Specifically, HOR reduces anodic operating cost by 5.7%, while SWITCH-R achieves a 19.6% reduction. Note that SWITCH-R requires plant oversizing to maintain a constant production rate, which increases capital cost.

SWITCH-NR provides only an additional 0.7% anodic cost reduction relative to SWITCH-R. Finally, TUNE achieves the largest anodic cost reduction (22.6%), which we attribute to operation at intermediate HOR/OER fractions and adjustment of energy demand to the electricity price. Importantly, the superiority of the tunable strategy over both SWITCH-R and SWITCH-NR indicates that the main value of the proposed architecture lies not only in transition management, but also in enabling continuous electrochemical load control.

Figure 4 highlights the key process-level advantage of the proposed concept: continuous tuning does not merely reproduce the benefit of binary switching, but extends flexible operation into intermediate electricity-price regimes. Whereas conventional switching strategies can only alternate between two discrete operating states, the tunable architecture allows anodic energy demand to more closely track the external price signal. As a result, the benefit of the present concept lies not only in eliminating rinsing-related downtime, but also in introducing a continuous control variable that improves economic responsiveness under realistic, gradually varying market conditions.

The anodic operating cost reduction depends on the assumed prices of hydrogen, deionized water, and electricity. Here, the H_2 price is treated as a delivered variable cost that includes major balance-of-plant contributions, whereas capital expenditures for dedicated high-pressure storage and site-specific infrastructure

3053786x, 2026, 1, Downloaded from https://advanced.onlinelibrary.wiley.com/doi/10.1002/ache.70003 by Universitatsbibliothek RWTH Aachen University, Wiley Online Library on [30/09/2026]. See the Terms and Conditions (https://onlinelibrary.wiley.com/terms-and-conditions) on Wiley Online Library for rules of use; OA articles are governed by the applicable Creative Commons License

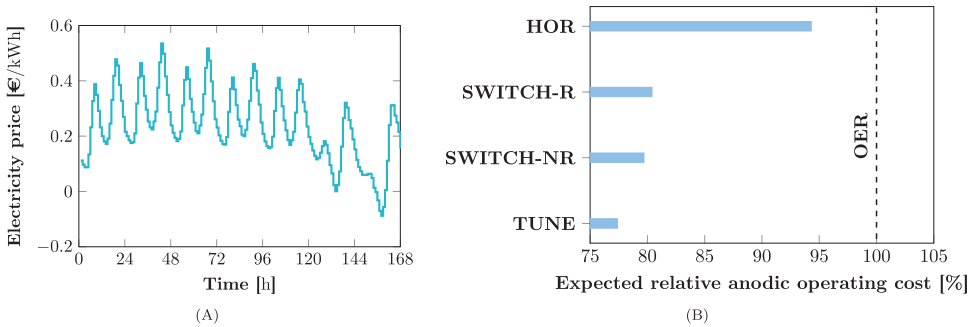


FIGURE 4 | (A) Representative weekly electricity-price profile for 2022 used for the comparative operating-cost analysis, adapted from Papadimitriou et al. [27]. (B) Relative anodic operating cost for different operating strategies, including HOR, switchable with rinsing (SWITCH-R), switchable without rinsing (SWITCH-NR), and tunable operation (TUNE), normalized to conventional OER operation (black dotted line). The tunable strategy yields additional cost savings over purely binary switching by allowing operation in intermediate electricity-price regimes.

are not modeled explicitly. Accordingly, Figure 4 should be interpreted as a comparative analysis of anodic operating-cost trends and of the relative benefit of switching and tuning under conservative price assumptions, rather than as a complete techno-economic assessment of hydrogen infrastructure.

The model is intended to capture the operating logic and process-level relevance of introducing a tunable anodic degree of freedom, rather than to provide a full process design or investment analysis. Even within this simplified comparative framework, the qualitative advantage of switchable and tunable operation remains robust across a broad range of plausible price scenarios. While the absolute magnitude of the cost reduction depends on the specific hydrogen and electricity prices, the ability to dynamically adjust the HOR/OER contribution enables the system to exploit both high-price and intermediate-price regimes more effectively than purely binary strategies. In particular, continuous tuning allows operation close to the break-even electricity price for hydrogen utilization; see Section S1 for a simple energetic bound for HOR-assisted voltage reduction and the corresponding break-even electricity price.

These assumptions provide a realistic scenario consistent with observed trends in electricity-price fluctuations and the emerging hydrogen economy. When evaluating total operating cost—including other contributors such as cathodic overpotentials or electrolyte costs—the reduction percentages are expected to differ. Moreover, the results were obtained assuming participation in the day-ahead electricity market. Participation in ancillary service markets, such as primary or secondary balancing power, could further improve the profitability of flexible operation strategies [40].

These findings highlight that the value of the proposed architecture lies not only in maximizing savings under extreme conditions, but also in maintaining favorable operation across realistic, time-varying market environments. Future work should extend this analysis to include capital expenditures, hydrogen storage strategies, and participation in ancillary service markets to fully quantify system-level benefits.

From an engineering perspective, the main relevance of the proposed architecture lies in its compatibility with electrochemical processes that require a fixed product-side operating point while benefiting from flexible power consumption. This includes, for example, CO_2 electrolysis, chlor–alkali electrolysis, and electrosynthesis platforms in which the desired reaction occurs at one electrode and the counter reaction primarily serves charge balancing. In such systems, the tunable-anode concept offers a route to dynamic load adaptation without relying exclusively on electrolyzer oversizing or product/intermediate storage.

Importantly, the superiority of the tunable strategy over both SWITCH-R and SWITCH-NR indicates that the main value of the proposed architecture lies not only in transition management but also in introducing continuous electrochemical load control.

Concerning scale-up, the present results should be interpreted as a first reactor-level demonstration of the operating principle. Translation to industrially relevant current densities will require optimization of membrane resistance, gas-distribution design, current collection, and thermal management in the dual-anode configuration. However, these challenges are engineering optimization tasks rather than conceptual barriers. The essential contribution of the present study is to establish that continuous control over the counter-electrode reaction split is experimentally feasible and process-relevant, thereby opening a new design space for flexible electrochemical reactor operation.

4 | Conclusion

In summary, we introduce a switchable and tunable two-chamber anode architecture that enables rinsing-free transitions between H_2 mode (HOR-anode) and O_2 mode (OER-anode), while also allowing continuous adjustment of their relative contributions. This design overcomes key limitations of conventional gas-switching concepts by eliminating downtime associated with inert-gas purging and enabling safe, simultaneous operation of both modes. As a result, the system provides a continuous "dial" to modulate cell voltage and power demand at constant cathodic current density, thereby decoupling energy consumption from production rate.

Experimentally, we demonstrate stable switching over 120 cycles at 100 mA cm^{-2} and tunable operation across the full 0%–100% HOR/OER range. Together with negligible O_2 crossover under the investigated conditions, these results establish the

3053786x, 2026, 1, Downloaded from https://advanced.onlinelibrary.wiley.com/doi/10.1002/ache.70003 by Universitatsbibliothek RWTH Aachen University, Wiley Online Library on [30/09/2026]. See the Terms and Conditions (https://onlinelibrary.wiley.com/terms-and-conditions) on Wiley Online Library for rules of use; OA articles are governed by the applicable Creative Commons License

practical feasibility of dynamic anodic control. Model-based analysis further indicates that tunable operation can reduce anodic operating costs by up to 22.6% under representative electricity-price scenarios.

Importantly, this work provides a first demonstration of a new operational principle for electrochemical systems: dynamic modulation of counter-electrode chemistry to tune power demand while maintaining the production-side operating point. Accordingly, we emphasize feasibility, controllability, and process relevance rather than maximizing current density or demonstrating long-term durability in an application-specific stack design.

Beyond the specific system studied here, the proposed electrode-architecture concept provides a general strategy for flexible electrochemical process design. Independent control of counter-electrode reactions creates new opportunities to integrate electrochemical technologies with fluctuating renewable electricity without relying on electrolyzer oversizing or product storage. This approach is transferable to a wide range of electrochemical platforms, including chlor–alkali electrolysis, CO_2 reduction, and electrosynthesis of H_2O_2, and thus represents a step toward more adaptive and energy-efficient electrified chemical processes.

Acknowledgments

M. Wessling acknowledges DFG funding through the Gottfried Wilhelm Leibniz Award 2019 (WE 4678/12-1). This work was supported by the German Federal Ministry of Education and Research (BMBF) under the project "HyInnoChem" (03ZU1115I) within the framework of the H_2-cluster and the project "iNEW 2.0" (03SF0627B). This work was conducted in part at the Competence Center for Industrial Electrochemistry ELECTRA, which is supported by the European Regional Development Fund (ERDF) and the Federal State of North Rhine-Westphalia (Grant No ERDF 05 00 07 7).

Open access funding enabled and organized by Projekt DEAL.

Conflicts of Interest

The authors declare no conflicts of interest.

Data Availability Statement

The data that support the findings of this study are available on request from the corresponding author. The data are not publicly available due to privacy or ethical restrictions.

References

1. L. C. Brée, K. Perrey, A. Bulan, and A. Mitsos, "Demand Side Management and Operational Mode Switching in Chlorine Production," *AIChE Journal* 65, no. 7 (2019): e16352.

2. K. Roh, L. C. Brée, K. Perrey, A. Bulan, and A. Mitsos, "Optimal Oversizing and Operation of the Switchable Chlor-Alkali Electrolyzer for Demand Side Management," in *Computer Aided Chemical Engineering*, Vol. 46 (Elsevier, 2019), 1771–1776.

3. B. Daryanian, R. E. Bohn, and R. D. Tabors, "Optimal Demand-Side Response to Electricity Spot Prices for Storage-Type Customers," *IEEE transactions on Power Systems* 4, no. 3 (1989): 897–903.

4. A. Ghobeity and A. Mitsos, "Optimal Time-Dependent Operation of Seawater Reverse Osmosis," *Desalination* 263, no. 1–3 (2010): 76–88.

5. J.-L. Gustin, "Safety of Chlorine Production and Chlorination Processes," *Chemical Health & Safety* 12, no. 1 (2005): 5–16.

6. L.-Y. Liang, J.-Y. Nie, Q. Wang, J.-F. Wu, and L. Chou, "Introduction and Safe Use of Gas Cylinders in China," *ACS Chemical Health & Safety* 31 (2024): 186–192.

7. A. Bulan, R. Weber, and F. Bienen, "Bifunktionelle Elektrode und Elektrolysevorrichtung für die Chlor-Alkali-Elektrolyse," (2017), international application PCT/EP2017/057956; filed 2017-04-04; priority 2016-04-07. [Online]. Available: https://patents.google.com/patent/WO2017174563A1/en.

8. K. Baitalow, N. Köller, P. Bacmeister, R. Keller, and M. Wessling, "On the Operation of Switchable Oxygen Depolarized Cathodes," *Chemical Engineering Journal* 469 (2023): 143759.

9. J. Jung, S. Postels, and A. Bardow, "Cleaner Chlorine Production Using Oxygen Depolarized Cathodes? A Life Cycle Assessment," *Journal of Cleaner Production* 80 (2014): 46–56.

10. P. Bai, V. Viswanathan, and M. Z. Bazant, "A Dual-Mode Rechargeable Lithium–Bromine/Oxygen Fuel Cell," *Journal of Materials Chemistry A* 3, no. 27 (2015): 165–14172.

11. B. You and Y. Sun, "Innovative Strategies for Electrocatalytic Water Splitting," *Accounts of Chemical Research* 51, no. 7 (2018): 1571–1580.

12. F. Faverjon, M. Rakib, and G. Durand, "Electrochemical Study of a Hydrogen Diffusion Anode-Membrane Assembly for Membrane Electrolysis," *Electrochimica Acta* 51, no. 3 (2005): 386–394.

13. F. Faverjon, G. Durand, and M. Rakib, "Regeneration of Hydrochloric Acid and Sodium Hydroxide From Purified Sodium Chloride by Membrane Electrolysis Using a Hydrogen Diffusion Anode-Membrane Assembly," *Journal of Membrane Science* 284, no. 1–2 (2006): 323–330.

14. J. Jörissen and K. H. Simmrock, "Behaviour of Ion-Exchange Membranes in Electrolysis and Electrodialysis of Sodium Sulphate," *Journal of Applied Electrochemistry* 21 (1991): 869–876.

15. M. Rakib, P. Moçotéguy, P. Viers, E. Petit, and G. Durand, "Hydrogen Diffusion Electrode in a Membrane Electrolysis Process to Produce Sulfuric Acid and Sodium Hydroxide From Sodium Sulphate," *Journal of Applied Electrochemistry* 29 (1999): 1439–1448.

16. C. Xia, Y. Xia, P. Zhu, L. Fan, and H. Wang, "Direct Electrosynthesis of Pure Aqueous H_2O_2 Solutions up to 20% by Weight Using a Solid Electrolyte," *Science* 366, no. 6462 (2019): 226–231.

17. G. C. da Silva, K. J. J. Mayrhofer, E. A. Ticianelli, and S. Cherevko, "Activity and Stability of Pt/Iro_2 Bifunctional Materials as Catalysts for the Oxygen Evolution/Reduction Reactions," *ACS Catalysis* 8 (2018): 2081–2092.

18. G. C. da Silva, K. J. J. Mayrhofer, E. A. Ticianelli, and S. Cherevko, "The Degradation of Pt/Iro_x Oxygen Bifunctional Catalysts," *Electrochimica Acta* 308 (2019): 400–409.

19. J. Durst, C. Simon, F. Hasche, and H. A. Gasteiger, "Hydrogen Oxidation and Evolution Reaction Kinetics on Carbon Supported Pt, Ir, Rh, and Pd Electrocatalysts in Acidic Media," *Journal of The Electrochemical Society* 162, no. 1 (2015): F190–F203.

20. J. Zheng, W. Sheng, Z. Zhuang, B. Xu, and Y. Yan, "Universal Dependence of Hydrogen Oxidation and Evolution Reaction Activity of Platinum-Group Metals on Ph and Hydrogen Binding Energy," *Science Advances* 2 (2016): e1501602.

21. Z. Liu, H. Yang, R. Kutz, and R. I. Masel, "CO_2 Electrolysis to CO and O_2 at High Selectivity, Stability and Efficiency Using Sustainion Membranes," *Journal of the Electrochemical Society* 165, no. 15 (2018): J3371.

22. S. Sen, S. M. Brown, M. Leonard, and F. R. Brushett, "Electroreduction of Carbon Dioxide to Formate at High Current Densities Using Tin and Tin Oxide Gas Diffusion Electrodes," *Journal of Applied Electrochemistry* 49 (2019): 917–928.

3053786x, 2026, 1, Downloaded from https://advanced.onlinelibrary.wiley.com/doi/10.1002/ache.70003 by Universitatsbibliothek RWTH Aachen University, Wiley Online Library on [30/09/2026]. See the Terms and Conditions (https://onlinelibrary.wiley.com/terms-and-conditions) on Wiley Online Library for rules of use; OA articles are governed by the applicable Creative Commons License

23. J. Baessler, M. Wehner, M. Mohseni, J. Neumann, M. Wessling, and R. Keller, "Feed and Bleed Operating Mode for Electrochemical Flow Cells: Challenges, Solutions and Practical Insights," *ChemElectroChem* 12 (2025): e202500034.

24. Gurobi Optimization, LLC, "Gurobi Optimizer Reference Manual," (2024), [Online]. Available: https://www.gurobi.com.

25. E. Zhao, G. Xia, Y. Li, J. Zhan, G. Yu, and Y. Wang, "Technoeconomic Assessment of Electrochemical Hydrogen Peroxide Production With Gas Diffusion Electrodes Under Scenarios Relevant to Practical Water Treatment," *ACS ES&T Engineering Journal* 3, no. 11 (2023): 1800–1812.

26. L. N. Appelhans, D. Zuccaccia, A. Kovacevic, et al., "An Anion-Dependent Switch in Selectivity Results From a Change of C—H Activation Mechanism in the Reaction of an Imidazolium Salt With $IrH_5(PPh_3)_2$," *Journal of the American Chemical Society* 127, no. 46 (2005): 16299–16311.

27. C. Papadimitriou, J. C. Schulze, and A. Mitsos, "A Practical Scenario Generation Method for Electricity Prices on Day-Ahead and Intraday Spot Markets," *Computers and Chemical Engineering* 199, no. 8 (2025): 109118, https://doi.org/10.1016/j.compchemeng.2025.109118.

28. ChemCoast, "Fahrplan zur Realisierung Einer Wind-Wasserstoff-Wirtschaft in der Region Unterelbe," accessed December 03, https://www.chemcoast.de/uploads/130812_ChemCoast_Windwasserstoff_Unterelbe.pdf.

29. Zhou, Yuanrong and Searle, Stephanie, "Cost of Renewable Hydrogen Produced Onsite at Hydrogen Refueling Stations in Europe,"accessed January 01, 2026, https://www.theicct.org.cn/wp-content/uploads/2025/03/fuels-eu-cost-renew-H-produced-onsite-H-refueling-stations-europe-feb22.pdf.

30. A. A. Topalov, S. Cherevko, A. R. Zeradjanin, J. C. Meier, I. Katsounaros, and K. J. J. Mayrhofer, "Towards a Comprehensive Understanding of Platinum Dissolution in Acidic Media," *Chemical Science* 5 (2014): 631–638.

31. G. C. da Silva, K. J. J. Mayrhofer, E. A. Ticianelli, and S. Cherevko, "Dissolution Stability: The Major Challenge in the Regenerative Fuel Cells Bifunctional Catalysis," *Journal of the Electrochemical Society* 165, no. 16 (2018): F1376–F1384.

32. K. C. Neyerlin, W. Gu, J. Jorne, and H. A. Gasteiger, "Determination of Catalyst Unique Parameters for the Oxygen Reduction Reaction in a Pemfc," *Journal of the Electrochemical Society* 153, no. 10 (2006): A1955.

33. H. T. Chung, D. A. Cullen, D. Higgins, et al., "Direct Atomic-Level Insight Into the Active Sites of a High-Performance PGM-Free ORR Catalyst," *Science* 357, no. 6350 (2017): 479–484.

34. J. Liang, Q. Xiang, W. Lei, et al., "Ferric Iron Reduction Reaction Electro-Fenton With Gas Diffusion Device: A Novel Strategy for Improvement of Comprehensive Efficiency in Electro-Fenton," *Journal of Hazardous Materials* 412 (2021): 125195.

35. M. Mohseni, D. Felder, K. Percin, et al., "Toward Decentralized Wastewater Treatment: A Flow-Through Module Using Microtubular Gas Diffusion Electrodes for Micropollutants Removal," *Journal of Hazardous Materials* 458 (2023): 131987.

36. T. Franz, G. Papakonstantinou, and K. Sundmacher, "Transient Hydrogen Crossover in Dynamically Operated PEM Water Electrolysis Cells-A Model-Based Analysis," *Journal of Power Sources* 559 (2023): 232582.

37. C. R. Wang, J. M. Stansberry, R. Mukundan, et al., "Proton Exchange Membrane (PEM) Water Electrolysis: Cell-Level Considerations for Gigawatt-Scale Deployment," *Chemical Reviews* 125, no. 3 (2025): 1257–1302.

38. E. J. Park, C. G. Arges, H. Xu, and Y. S. Kim, "Membrane Strategies for Water Electrolysis," *ACS Energy Letters* 7, no. 10 (2022): 3447–3457.

39. S. Fahr, F. K. Engel, S. Rehfeldt, A. Peschel, and H. Klein, "Overview and Evaluation of Crossover Phenomena and Mitigation Measures in Proton Exchange Membrane (PEM) Electrolysis," *International Journal of Hydrogen Energy* 68 (2024): 705–721, https://doi.org/10.1016/j.ijhydene.2024.04.248.

40. P. Schäfer, H. G. Westerholt, A. M. Schweidtmann, S. Ilieva, and A. Mitsos, "Model-Based Bidding Strategies on the Primary Balancing Market for Energy-Intense Processes," *Computers & Chemical Engineering* 120 (2019): 4–14.

Supporting Information

Additional supporting information can be found online in the Supporting Information section.

Supporting File: ache70003-sup-0001-SuppMat.pdf.

30537986, 2026, 1, Downloaded from https://advanced.onlinelibrary.wiley.com/doi/10.1002/ache.70003 by Universitatsbibliothek RWTH Aachen University, Wiley Online Library on [30/09/2026]. See the Terms and Conditions (https://onlinelibrary.wiley.com/terms-and-conditions) on Wiley Online Library for rules of use; OA articles are governed by the applicable Creative Commons License